

Experimental test of the Crooks fluctuation theorem in a single nuclear spinWei Cheng,^{1,2} Wenquan Liu³, Zhibo Niu,^{1,2} Chang-Kui Duan,^{1,2,4} Xing Rong^{1,2,4,*} and Jiangfeng Du^{1,2,4,5,†}¹CAS Key Laboratory of Microscale Magnetic Resonance and School of Physical Sciences, University of Science and Technology of China, Hefei 230026, China²CAS Center for Excellence in Quantum Information and Quantum Physics, University of Science and Technology of China, Hefei 230026, China³School of Science, Beijing University of Posts and Telecommunications, Beijing 100876, China⁴Hefei National Laboratory, University of Science and Technology of China, Hefei 230088, China⁵School of Physics, Zhejiang University, Hangzhou 310027, China

(Received 25 November 2022; accepted 16 January 2024; published 20 February 2024)

We experimentally test the Crooks fluctuation theorem in a quantum spin system. Our results show that the Crooks fluctuation theorem is valid for different speeds of the nonequilibrium processes and under various effective temperatures. Work is not an observable in quantum systems, which makes tests of quantum thermodynamic theorems challenging. In this work, we develop high-fidelity single-shot readouts of a single nuclear spin in diamond and implement the two-point work measurement protocol, enabling a direct experimental test of the Crooks fluctuation theorem. Our results provide quantum insight into fluctuations and the methods we develop can be utilized to study other quantum thermodynamic theorems.

DOI: [10.1103/PhysRevA.109.L020401](https://doi.org/10.1103/PhysRevA.109.L020401)

Introduction. Fluctuations become prominent when the study of thermodynamics shifts from the macroscopic to the microscopic scale. These fluctuations can be comparable to ensemble averages of corresponding thermodynamic quantities [1] and are not mere background noises [2]. The investigation of these fluctuations has led to the discovery of various fluctuation theorems [3–7]. One important example is the Crooks fluctuation theorem (CFT) [8], which reads $P^F(W)/P^R(-W) = e^{\beta(W-\Delta F)}$, with β the inverse temperature. The CFT relates the probability $P^F(W)$ of performing some work W during a forward process to the probability $P^R(-W)$ of extracting the same amount of work during the time-reversed process via the free-energy difference ΔF , providing knowledge of far-from-equilibrium thermodynamics.

The CFT has been verified in several classical systems [9–12], but a direct test in quantum systems remains elusive. The difficulty originates from the fact that work is not an observable in the quantum realm [13]. For isolated quantum systems, the work done during a process can be measured by the two-point measurement (TPM) protocol [4,5]. The TPM protocol requires two high-fidelity nondemolition projective measurements on the energy basis at the start and the end of the process to determine work. Projective measurements with poor readout fidelity may not be able to obtain the initial and final energies correctly. Measurements that are not nondemolition will result in the state after measurement being different from the corresponding eigenstate. Such situations will lead to incorrect work distribution and unable to recover the CFT [14]. However, experimental realization of high-fidelity nondemolition projective measurement is

generally challenging. To evade the difficulty, some alternative but indirect approaches were proposed [15,16] to obtain the work distribution and were adopted in several experiments. In a liquid-state nuclear magnetic resonance setup, the work distribution was reconstructed by a characteristic function which was measured using an auxiliary qubit [17,18]. In addition, a presampling method was utilized to test some integral fluctuation theorems in the nitrogen-vacancy (NV) center system [19–21]. To date, an experiment that faithfully implements the TPM protocol to test the CFT is still absent.

Here we report an experimental test of the CFT in a single nuclear spin, i.e., the ^{14}N nuclear spin of the NV center in diamond. To implement the TPM protocol, high-fidelity nondemolition projective measurements of the ^{14}N nuclear spin are realized based on the single-shot readout technique [22]. The work statistics in the forward and time-reversed switching processes are experimentally obtained with the TPM protocol. Our results demonstrate that the obtained work statistics satisfy the CFT for various speeds of the switching process and for different effective temperatures of the initial thermal state.

Theory. To test the CFT, work distributions of an isolated quantum system undergoing the forward and corresponding time-reversed switching processes are measured via the TPM protocol. The procedure to obtain the work distribution in the forward switching process is shown in Fig. 1(a). First, the system is prepared in the thermal state of $H(0)$, $\rho_{\text{thm}}^0 = e^{-\beta H(0)}/Z^0$, with $Z^0 = \text{Tr}(e^{-\beta H(0)})$ the partition function. Then the first projective measurement is performed, projecting the system onto an energy eigenstate of $H(0)$, such as $|n\rangle$, with probability $p_n^0 = \text{Tr}(\rho_{\text{thm}}^0 |n\rangle\langle n|)$. Next the system undergoes the forward switching process. During this process, the Hamiltonian varies from $H(0)$ to $H(\tau)$ in a period of τ . The time-dependent Hamiltonian drives the system, for example, from $|n\rangle\langle n|$ into ρ_n^τ . Finally, the

*xrong@ustc.edu.cn

†djf@ustc.edu.cn

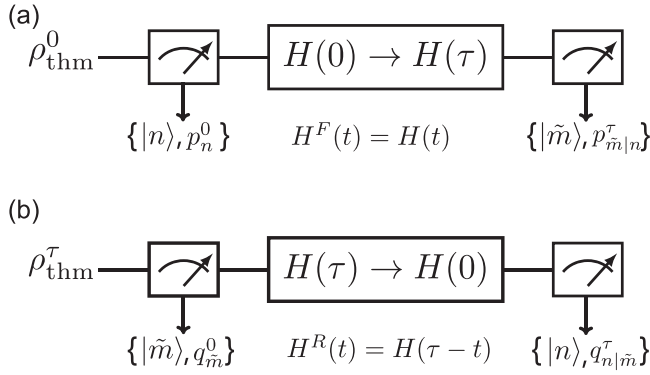


FIG. 1. The TPM protocol to obtain work distributions. (a) The forward switching process ρ_{thm}^0 is a thermal state of $H(0)$. The first and second projective measurements were performed at energy eigenstates of $H(0)$ and $H(\tau)$, respectively. (b) Corresponding time-reversed switching process. Here ρ_{thm}^τ is a thermal state of $H(\tau)$. The first and second projective measurements were performed at the energy eigenstates of $H(\tau)$ and $H(0)$, respectively.

second projective measurement is performed, projecting the system onto an energy eigenstate of $H(\tau)$, such as $|\tilde{m}\rangle$, and the corresponding probability is $p_{\tilde{m}|n}^\tau = \text{Tr}(\rho_n^\tau |\tilde{m}\rangle\langle\tilde{m}|)$. Then the work done on the system for trajectory $|n\rangle \rightarrow |\tilde{m}\rangle$ is obtained as $W_{\tilde{m}|n} = E_{\tilde{m}}^\tau - E_n^0$, with $E_{\tilde{m}}^\tau$ and E_n^0 the eigenenergies of states $|\tilde{m}\rangle$ and $|n\rangle$, respectively. The work distribution in the forward switching process can be represented as $P^F(W) = \sum_{\tilde{m},n} p_n^0 p_{\tilde{m}|n}^\tau \delta(W - W_{\tilde{m}|n})$. The corresponding time-reversed switching process is displayed in Fig. 1(b). The system is initially prepared in the thermal state of $H(\tau)$, $\rho_{\text{thm}}^\tau = e^{-\beta H(\tau)}/Z^\tau$, with $Z^\tau = \text{Tr}(e^{-\beta H(\tau)})$. The Hamiltonian is tuned from $H(\tau)$ to $H(0)$ in the time-reversed manner $H^R(t) = H(\tau - t)$. The work distribution in the time-reversed switching process can be represented as $P^R(W) = \sum_{\tilde{m},n} q_{\tilde{m}}^0 q_{n|\tilde{m}}^\tau \delta(W - W_{n|\tilde{m}})$. The left-hand side of the CFT, $P^F(W)/P^R(-W)$, can then be calculated from the obtained work distributions in the forward and time-reversed processes. The right-hand side of the CFT, $e^{\beta(W-\Delta F)}$, can be obtained via the Hamiltonian model $H(t)$ and the inverse

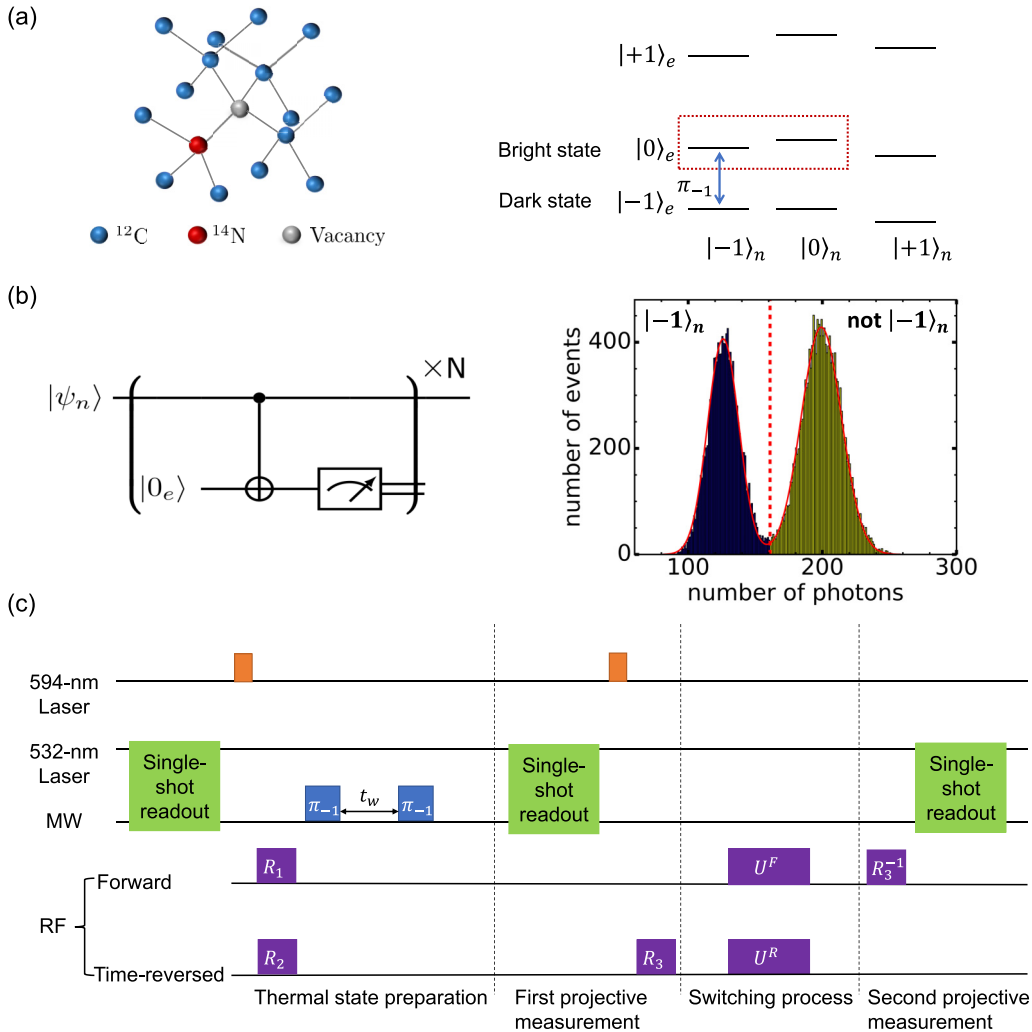


FIG. 2. Single-shot readout of the nuclear spin and realizing TPM in an NV center. (a) Atomic structure and ground-state energy levels of the NV center. The two energy levels in the red dotted box are utilized to test the CFT. (b) Single-shot readout. Shown on the left is the pulse sequence of single-shot readout, here $N = 1500$, and on right is the photon-counting histogram obtained by repeating single-shot readout. (c) Experimental pulse sequences to realize TPM to test the CFT.

temperature β . The CFT is tested by checking whether the difference $\Delta = P^F(W)/P^R(-W) - e^{\beta(W-\Delta F)}$ equals zero for all possible W .

Experiments. In our experiment, a single nuclear spin of the NV center was utilized to test the CFT. The NV center is a type of defect in diamond consisting of a substitutional nitrogen atom adjacent to a carbon vacancy. The left-hand side of Fig. 2(a) shows the atomic structure and ground-state energy levels of the NV center. When a magnetic field is applied along the symmetry axis of the NV center, the ground-state Hamiltonian can be written as

$$H_{\text{NV}} = 2\pi\hbar(DS_z^2 + \omega_e S_z + QI_z^2 + \omega_n I_z + A_{zz}I_z S_z), \quad (1)$$

where S_z and I_z are the spin operators of the NV electron spin and ^{14}N nuclear spin, respectively. The ground-state zero-field splitting of the electron spin is $D = 2.87$ GHz and the quadrupolar interaction of the nuclear spin is $Q = -4.95$ MHz. The longitudinal hyperfine interaction between nuclear spin and electron spin is $A_{zz} = -2.16$ MHz. The Zeeman frequencies of the electron and nuclear spin induced by the external static magnetic field are denoted by ω_e and ω_n , respectively. The electron spin can be polarized into $|0\rangle_e$ via a spin-selective intersystem crossing process [23]. Due to the same mechanism, the photoluminescence rate for $|0\rangle_e$ is higher than that for $|-1\rangle_e$. In the following, we denote by $|0\rangle_e$ the bright state and by $|-1\rangle_e$ the dark state. Two energy levels of the ^{14}N nuclear spin, $|-1\rangle_n$ and $|0\rangle_n$, are chosen to form a two-level system to test the CFT as shown by the red dotted box in Fig. 2(a).

High-fidelity nondemolition projective measurement of the nuclear spin is realized via the single-shot readout technique. The single-shot readout process is displayed in Fig. 2(b). The electron spin is optically pumped into the bright state. Then a selective π_{-1} pulse flips the electron spin to the dark state on the condition that the nuclear spin state is $|-1\rangle_n$. Next a 532-nm laser pulse is applied to read out the electron spin and repolarize it to the bright state. By repeating this procedure, a fluorescence signal can be accumulated to read out the nuclear spin. In the ideal case, the nuclear spin can be projectively measured. In practice, the projected state could be altered during the readout process due to the nuclear spin relaxation [22]. To suppress the relaxation, we apply a static magnetic field of approximately 7500 G along the NV symmetry axis. In addition, the imperfection of the selective π_{-1} pulse will also corrupt the fidelity. Thus, a noise-robust gate is designed via an optimal control method. The repetition number N is also appropriately chosen to optimize the fidelity. With these techniques, the optimized fidelity achieves 0.98(1) (see Appendix A for details). To realize projective measurements along arbitrary energy bases, necessary rotations can be applied before and after the single-shot readout.

The experimental pulse sequences are depicted in Fig. 2(c). By performing the single-shot readout and postselecting the states with fluorescence below the threshold, the nuclear spin can be initialized into $|-1\rangle_n$. During the readout process, the applied 532-nm laser pulse can induce transitions between two charge states NV^0 and NV^- of the NV center. A 594-nm laser pulse is applied to postselect the experiment trials done with NV^- [24]. In this work, the Hamiltonian of the switching

process is chosen as

$$\begin{aligned} H^F(t) &= 2\pi\hbar[Z(t)S'_z + X(t)S'_x], \\ H^R(t) &= 2\pi\hbar[Z(\tau-t)S'_z + X(\tau-t)S'_x], \end{aligned} \quad (2)$$

with $S'_z = (|1\rangle\langle 1| - |0\rangle\langle 0|)/2$, $S'_x = (|1\rangle\langle 0| + |0\rangle\langle 1|)/2$, $Z(t) = 2$ kHz, and $X(t) = 5[1 - \cos(\pi t/\tau)]/2$ kHz. Here and in the following, for convenience, the energy levels $|0\rangle_n$ and $|-1\rangle_n$ are relabeled as $|1\rangle$ and $|0\rangle$, respectively. The thermal state of $H(0)$ is generated in two steps. In the first step, a resonant radio-frequency pulse R_1 is applied to prepare the state $\sqrt{P_{\text{thm}}^0}|0\rangle + \sqrt{P_{\text{thm}}^1}|1\rangle$, where P_{thm} is the thermal population. In the second step, two selective π_{-1} pulses separated by a waiting time $t_w = 10$ μs are applied to dissipate the coherence. The coherence dissipates quickly as the dephasing time of the electron spin $T_{2,e}^* < 1.5$ μs . After the preparation of the thermal state, the first projective measurements are performed to project the system onto energy eigenstates. In the time-reversed process, the eigenstates of $H(0)$ differ from the computational basis, so an additional rotation pulse R_3 is applied after the single-shot readout. Then the time-dependent Hamiltonian or its time-reversed counterpart is applied to change the system state. Some work is extracted from or performed on the system during the switching process. Finally, the second projective measurements are performed to obtain the work trajectories. In the forward process, the eigenstates of $H(\tau)$ differ from the computational basis, so an additional rotation pulse R_3^{-1} is applied before the single-shot readout. To obtain the work statistics, the pulse sequence is executed 16 000 times for each experimental data point. The postselection ratios for the nuclear state initialization and charge state selection are 32% and 41%, respectively. Since the charge state postselection is executed twice in our experimental sequence, the total success ratio is about 5.4%. By analyzing the postselected data, we can obtain the work statistics of these switching processes.

To test the CFT in switching processes with different degrees of adiabaticity, we conduct the experimental investigations with switching time τ ranging from 25 to 300 μs . The adiabaticity can be evaluated by the parameter [25] $\Gamma = \min_{t \in [0, \tau]} | \langle n_1(t) | \partial H(t) / \partial t | n_2(t) \rangle | / [E_1(t) - E_2(t)]^2$. Here $|n_1(t)\rangle$ and $|n_2(t)\rangle$ are two instantaneous eigenstates of $H(t)$, with $E_1(t)$ and $E_2(t)$ the corresponding energies. When Γ is much smaller than 1, the switching process can be considered adiabatic. In our experiment, the switching process varies from a fast process to a close-to-adiabatic process with Γ decreasing from 3.6 to 0.3. The experimental probability distributions of trajectories in the forward process and corresponding time-reversed process are displayed in Figs. 3(a) and 3(b), respectively. Here P_{ij}^F refers to the probability of the trajectory $|i\rangle \rightarrow |\tilde{j}\rangle$ in the forward process and P_{ji}^R refers to the probability of the trajectory $|\tilde{j}\rangle \rightarrow |i\rangle$ in the time-reversed process. The error bars shown here represent the 95% confidence interval. As τ increases, the transition probabilities between different instantaneous eigenstates decrease, indicating that the process is approaching the adiabatic regime gradually. To calculate the differences $\Delta_{ij} = P_{ij}^F / P_{ji}^R - e^{\beta(W_{ij} - \Delta F)}$, the effective inverse temperature β_{expt} and free-energy difference ΔF are obtained from the

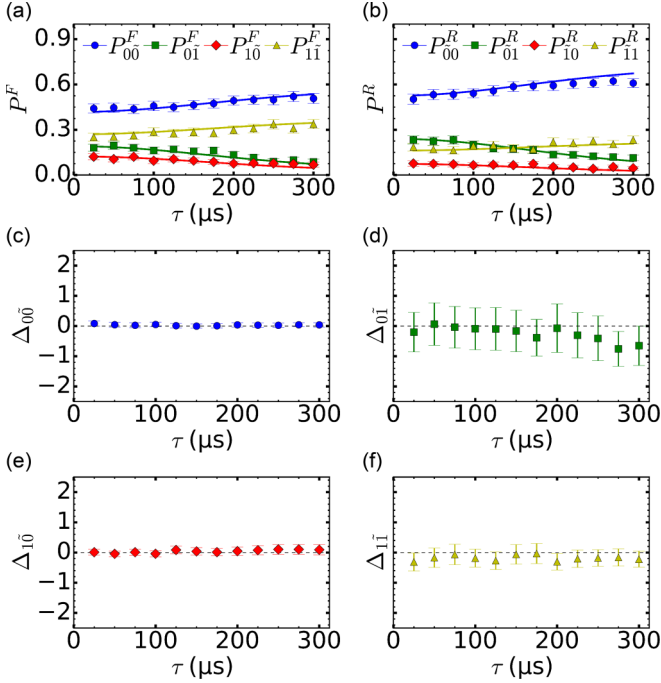


FIG. 3. Experimental verification of the CFT for different switching times. Probability distributions of trajectories are shown in (a) the forward processes and (b) the corresponding time-reversed processes for different switching times. [(c)–(f)] Test of the CFT utilizing different trajectories. Dots with error bars show $\Delta_{ij} = P_{ij}^F/P_{ji}^R - e^{\beta(W_{ij}-\Delta F)}$ for different switching times.

measured initial thermal populations (see Appendix B for details). Experimentally, the same initial thermal state is prepared for each switching time. However, mainly due to the single-shot noises, the measured populations have nonzero uncertainties, leading to uncertainty in the value of β_{expt} . Here the effective inverse temperature is $h\beta_{\text{expt}} = 0.22(3) \text{ kHz}^{-1}$. The uncertainties of Δ_{ij} are obtained utilizing the error transfer formula. As displayed in Fig. 3(d), the uncertainties of Δ_{10} are considerably larger than those of the other three, mainly because the denominator P_{10}^R in Δ_{10} is considerably smaller. As shown by Figs. 3(c)–3(f), these experimental points can be considered equal to zero when error bars are taken into account, confirming the validity of the CFT for different speeds of the switching process.

Furthermore, to test the CFT under different temperatures, we prepare different initial thermal states. Our experiment fixes the switching time at $\tau = 25 \mu\text{s}$. The inverse temperatures are preset as $h\beta = 0, 0.15, 0.25, 0.35 \text{ kHz}^{-1}$, with $h\beta = 0 \text{ kHz}^{-1}$ representing an infinitely high temperature. The effective inverse temperatures are $h\beta_{\text{expt}} = 0.03(3), 0.15(3), 0.27(3), 0.36(4) \text{ kHz}^{-1}$. For different effective temperatures, the difference Δ_{ij} and their uncertainties are calculated. As shown by Figs. 4(a)–4(d), these experimental points can be considered as equal to zero when error bars are taken into account, verifying the CFT under different temperatures.

Conclusion. We have experimentally tested the CFT by faithfully implementing the TPM protocol. The work distributions in the forward and corresponding time-reversed

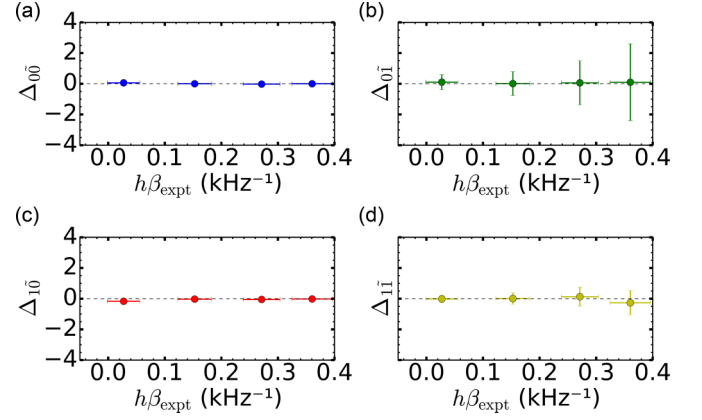


FIG. 4. Experimental verification of the CFT under different temperatures. The test of the CFT is shown utilizing different trajectories. Dots with vertical error bars show $\Delta_{ij} = P_{ij}^F/P_{ji}^R - e^{\beta(W_{ij}-\Delta F)}$ for different effective temperatures. The horizontal error bars represent the errors of $h\beta_{\text{expt}}$.

switching processes were measured and the difference between the left- and right-hand sides of the CFT was obtained. The experimental results show that the difference is zero for different speeds of nonequilibrium processes and under various effective temperatures, providing a rigorous validation of the CFT. Additionally, our development of high-fidelity nondemolition projective measurement in the NV center system can facilitate the investigation of quantum thermodynamics, enabling us to study many other important thermodynamic principles and interesting phenomena. For example, the fluctuation theorem in the non-Hermitian regime [26], information-theoretic-based quantum thermodynamics [27,28], and quantum thermodynamic devices [29–31] can be explored further. It should be noted that the TPM protocol has been regarded to destroy quantum features [32]. Recently, in bipartite systems, fluctuations of heat exchange were studied beyond the framework of the TPM protocol to consider the influence of quantum correlation [33,34]. There have also been other attempts to explore alternative measurement protocols [35–37] that account for initially coherent states. However, in our test of the quantum CFT, the system needs to be prepared in a thermal state with no quantum coherence or quantum correlation, and therefore the TPM protocol is an appropriate and standard method.

Acknowledgments. We thank Y. Wu for helpful discussions. This work was supported by the National Key R&D Program of China (Grants No. 2018YFA0306600 and No. 2016YFB0501603), the National Natural Science Foundation of China (Grant No. 12174373), the Chinese Academy of Sciences (Grants No. XDC07000000 and No. GJJSTD20200001), Innovation Program for Quantum Science and Technology (Grant No. 2021ZD0302200), Anhui Initiative in Quantum Information Technologies (Grant No. AHY050000), and Hefei Comprehensive National Science Center. X.R. is grateful to the Youth Innovation Promotion Association of Chinese Academy of Sciences for their support. W.L. was funded by Beijing University of Posts and Telecommunications Innovation Group.

W.C. and W.L. contributed equally to this work.

TABLE I. Effective inverse temperatures and corresponding initial populations of forward and time-reversed process. Here $h\beta_{\text{expt}}^F$ and $h\beta_{\text{expt}}^R$ were obtained from initial populations; $h\beta_{\text{expt}}$ was obtained as $h\beta_{\text{expt}} = (h\beta_{\text{expt}}^F + h\beta_{\text{expt}}^R)/2$

$h\beta_{\text{expt}}$	p_0	p_1	$h\beta_{\text{expt}}^F$	q_0	q_1	$h\beta_{\text{expt}}^R$
0.03(3)	0.52(4)	0.48(4)	0.04(4)	0.53(4)	0.47(4)	0.02(2)
0.15(3)	0.58(4)	0.42(4)	0.16(5)	0.69(4)	0.31(4)	0.15(2)
0.27(3)	0.63(4)	0.37(4)	0.27(6)	0.81(3)	0.19(3)	0.27(3)
0.36(4)	0.68(4)	0.32(4)	0.38(6)	0.86(3)	0.14(3)	0.34(4)

Appendix A: High-Fidelity Projective Measurement. To improve the fidelity, the measurement backaction should be mitigated and the detection efficiency should be improved. We applied a static magnetic field of about 7500 G along the NV symmetry axis to mitigate the measurement backaction. We created a solid immersion lens [38] in the diamond and used an oil objective to improve the detection efficiency. Furthermore, the optimal control method [39] was utilized to realize a noise-robust gate in the single-shot readout.

We studied the optimal quantum control in the Hilbert space spanned by $|1\rangle_n|0\rangle_e$, $|0\rangle_n|0\rangle_e$, $|-1\rangle_n|0\rangle_e$, $|1\rangle_n|-1\rangle_e$, $|0\rangle_n|-1\rangle_e$, and $|-1\rangle_n|-1\rangle_e$. Microwave pulses, whose frequency equals the energy difference between $|0\rangle_n|0\rangle_e$ and $|-1\rangle_n|0\rangle_e$, were applied to control the NV electron spin. In the rotational frame, the system Hamiltonian is $H_0 = 2\pi A_{zz}I_z \otimes |-1\rangle_e\langle -1|$. The control Hamiltonian is a piecewise constant. Defining $t_i = t_0 + i\Delta t$, the control Hamiltonian at $t \in [t_{i-1}, t_i)$ takes the form

$$H_c(t) = 2\pi[\Omega_x(t)H_x + \Omega_y(t)H_y] = 2\pi(\Omega_{ix}H_x + \Omega_{iy}H_y), \quad (\text{A1})$$

where Ω_{ix} and Ω_{iy} are parameters to be optimized and $H_{x,y} = \mathbf{1}_n \otimes S'_{x,y}$. The amplitude noise of the control field leads to $H_c(t) = (1 + \alpha)H_c(t)$ and the static dephasing noise takes the form $H_d = \mathbf{1}_n \otimes 2\pi\delta S'_z$. The total Hamiltonian is $H(t) = H_0 + (1 + \alpha)H_c(t) + H_d$. The evolution time is set as $T = 4/|A_{zz}|$ and is divided into $M = 10$ segments of equal length. The propagator of these pulses is $U(T) = \Pi_i e^{-jH_i T/M}$, where $H_i = H_0 + (1 + \alpha)[2\pi(\Omega_{ix}H_x + \Omega_{iy}H_y)] + H_d$. The target gate is $U_{\text{targ}} = |-1\rangle_n\langle -1| \otimes e^{-j\pi S'_x} + (|1\rangle_n\langle 1| + |0\rangle_n\langle 0|) \otimes \mathbf{1}_e$. The fidelity between U and U_{targ} is defined as $\mathcal{F} = |\text{Tr}(U_{\text{targ}}^\dagger U)|^2 / \text{Tr}(U_{\text{targ}}^\dagger U_{\text{targ}})$. We designed a noise-robust pulse that can realize a high-fidelity U with arbitrary α and δ , where $\alpha \in [\alpha_{\min}, \alpha_{\max}]$ and $\delta \in [\delta_{\min}, \delta_{\max}]$. The pulse shape and its robustness are shown in Figs. 5(a) and 5(b), respectively.

Photon-counting histograms and fluorescence time traces with both an optimized pulse and a naive square-wave pulse are shown in Figs. 5(c)–5(f). In the fluorescence time trace, each data point was acquired by the single-shot readout with repetition number $N = 1500$ (total time 9 ms). There is a telegraphlike signal in the fluorescence time trace, and two plateaus represent that the nuclear spin stays in or does not stay in $|-1\rangle_n$. The transition between the two plateaus comes from either misjudgment or intrinsic flips of the nuclear spin. The average data point of the nuclear spin being in $|-1\rangle_n$ is \bar{n}_0 and the nuclear spin not being

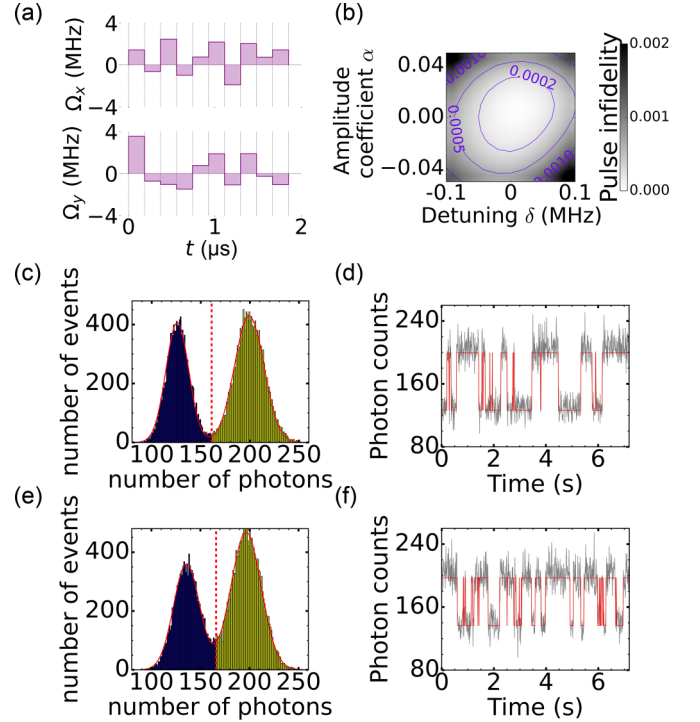


FIG. 5. Single-shot readout with optimal control. (a) Optimized pulse and (b) its robustness to noise. The photon-counting histogram and fluorescence time trace are shown with (c) and (d) an optimized pulse and (e) and (f) a naive square-wave pulse.

in $|-1\rangle_n$ is \bar{n}_1 . The fidelity can be defined as $(F_{0,1})^2 = 1 - 1/\bar{n}_{0,1}$. In our experiment $\bar{n}_{0,1} \gg 1$ and the average fidelity is approximately

$$F = 1 - \frac{1}{2} \left(\frac{1}{2\bar{n}_0} + \frac{1}{2\bar{n}_1} \right). \quad (\text{A2})$$

Fidelities with an optimized pulse and a naive square wave pulse are $F_{\text{opt}} = 0.98(1)$ and $F_{\text{sq}} = 0.96(1)$, respectively.

Appendix B: Calculation of β_{expt} and ΔF . Utilizing a single two-level system, four potential work trajectories exist during a switching process in our experiment. The work distribution and its uncertainty were obtained by counting these four trajectories. The effective inverse temperature β_{expt} and its error were calculated by the work distribution and its uncertainty. For convenience, we denote $P^F(W = E_j^\tau - E_i^0)$ by P_{ij}^F in the following. To obtain β_{expt} , we calculated the initial population p_i by summing P_{ij}^F over the index j , $p_i = \sum_j P_{ij}^F$. In the forward process, β_{expt}^F is given by $\beta_{\text{expt}}^F = \ln(p_0/p_1)/(E_1^0 - E_0^0)$ and its error can be calculated using error transfer formula. In the time-reversed process, β_{expt}^R and its error were obtained similarly. The average effective inverse temperature is $\beta_{\text{expt}} = (\beta_{\text{expt}}^F + \beta_{\text{expt}}^R)/2$. Upon obtaining β_{expt} , the free-energy difference can be calculated as $\Delta F = -\ln[\text{Tr}(e^{-\beta_{\text{expt}}H(\tau)})/\text{Tr}(e^{-\beta_{\text{expt}}H(0)})]/\beta_{\text{expt}}$. In the test of the CFT for different speeds of switching processes, the effective inverse temperature was $h\beta_{\text{expt}} = 0.22(3) \text{ kHz}^{-1}$, with $h\beta_{\text{expt}}^F = 0.24(5) \text{ kHz}^{-1}$ and $h\beta_{\text{expt}}^R = 0.20(2) \text{ kHz}^{-1}$. In

the test of the CFT under different temperatures, $h\beta_{\text{expt}}$ and corresponding initial populations are listed in Table I. The

errors of $h\beta_{\text{expt}}^R$ are smaller than $h\beta_{\text{expt}}^F$ due to the larger energy gap of $H(\tau)$ than $H(0)$.

-
- [1] E. Bäumer, M. Lostaglio, M. Perarnau-Llobet, and R. Sampaí, Fluctuating work in coherent quantum systems: Proposals and limitations, in *Thermodynamics in the Quantum Regime*, edited by F. Binder, L. Correa, C. Gogolin, J. Anders, and G. Adesso, Fundamental Theories of Physics Vol. 195 (Springer, Cham, 2018), pp. 275–300.
- [2] C. Jarzynski, Equalities and inequalities: Irreversibility and the second law of thermodynamics at the nanoscale, *Annu. Rev. Condens. Matter Phys.* **2**, 329 (2011).
- [3] E. Sevick, R. Prabhakar, S. R. Williams, and D. J. Searles, Fluctuation theorems, *Annu. Rev. Phys. Chem.* **59**, 603 (2008).
- [4] M. Esposito, U. Harbola, and S. Mukamel, Nonequilibrium fluctuations, fluctuation theorems, and counting statistics in quantum systems, *Rev. Mod. Phys.* **81**, 1665 (2009).
- [5] M. Campisi, P. Hänggi, and P. Talkner, *Colloquium*: Quantum fluctuation relations: Foundations and applications, *Rev. Mod. Phys.* **83**, 771 (2011).
- [6] K. Funo, M. Ueda, and T. Sagawa, Quantum fluctuation theorems, in *Thermodynamics in the Quantum Regime*, edited by F. Binder, L. Correa, C. Gogolin, J. Anders, and G. Adesso, Fundamental Theories of Physics Vol. 195 (Springer, Cham, 2018), pp. 249–273.
- [7] G. T. Landi and M. Paternostro, Irreversible entropy production: From classical to quantum, *Rev. Mod. Phys.* **93**, 035008 (2021).
- [8] G. E. Crooks, Entropy production fluctuation theorem and the nonequilibrium work relation for free energy differences, *Phys. Rev. E* **60**, 2721 (1999).
- [9] S. Schuler, T. Speck, C. Tietz, J. Wrachtrup, and U. Seifert, Experimental test of the fluctuation theorem for a driven two-level system with time-dependent rates, *Phys. Rev. Lett.* **94**, 180602 (2005).
- [10] D. Collin, F. Ritort, C. Jarzynski, S. B. Smith, I. Tinoco, and C. Bustamante, Verification of the Crooks fluctuation theorem and recovery of RNA folding free energies, *Nature (London)* **437**, 231 (2005).
- [11] I. Junier, A. Mossa, M. Manosas, and F. Ritort, Recovery of free energy branches in single molecule experiments, *Phys. Rev. Lett.* **102**, 070602 (2009).
- [12] O.-P. Saira, Y. Yoon, T. Tanttu, M. Möttönen, D. V. Averin, and J. P. Pekola, Test of the Jarzynski and Crooks fluctuation relations in an electronic system, *Phys. Rev. Lett.* **109**, 180601 (2012).
- [13] P. Talkner, E. Lutz, and P. Hänggi, Fluctuation theorems: Work is not an observable, *Phys. Rev. E* **75**, 050102(R) (2007).
- [14] P. Hänggi, and P. Talkner, The other QFT, *Nat. Phys.* **11**, 108 (2015).
- [15] L. Mazzola, G. De Chiara, M. Paternostro, D. V. Averin, and J. P. Pekola, Measuring the characteristic function of the work distribution, *Phys. Rev. Lett.* **110**, 230602 (2013).
- [16] R. Dorner, S. R. Clark, L. Heaney, R. Fazio, J. Goold, and V. Vedral, Extracting quantum work statistics and fluctuation theorems by single-qubit interferometry, *Phys. Rev. Lett.* **110**, 230601 (2013).
- [17] T. B. Batalhão, A. M. Souza, L. Mazzola, R. Aucaise, R. S. Sarthour, I. S. Oliveira, J. Goold, G. De Chiara, M. Paternostro, and R. M. Serra, Experimental reconstruction of work distribution and study of fluctuation relations in a closed quantum system, *Phys. Rev. Lett.* **113**, 140601 (2014).
- [18] T. B. Batalhão, A. M. Souza, R. S. Sarthour, I. S. Oliveira, M. Paternostro, E. Lutz, and R. M. Serra, Irreversibility and the arrow of time in a quenched quantum system, *Phys. Rev. Lett.* **115**, 190601 (2015).
- [19] S. Hernández-Gómez, A. M. Souza, R. S. Sarthour, I. S. Oliveira, M. Paternostro, E. Lutz, and R. M. Serra, Experimental test of exchange fluctuation relations in an open quantum system, *Phys. Rev. Res.* **2**, 023327 (2020).
- [20] S. Hernández-Gómez, N. Staudenmaier, M. Campisi, and N. Fabbri, Experimental test of fluctuation relations for driven open quantum systems with an NV center, *New J. Phys.* **23**, 065004 (2021).
- [21] S. Hernández-Gómez, S. Gherardini, N. Staudenmaier, F. Poggiali, M. Campisi, A. Trombettoni, F. Cataliotti, P. Cappellaro, and N. Fabbri, Autonomous dissipative Maxwell’s demon in a diamond spin qutrit, *PRX Quantum* **3**, 020329 (2022).
- [22] P. Neumann, J. Beck, M. Steiner, F. Rempp, H. Fedder, P. R. Hemmer, J. Wrachtrup, and F. Jelezko, Single-shot readout of a single nuclear spin, *Science* **329**, 542 (2010).
- [23] V. Jacques, P. Neumann, J. Beck, M. Markham, D. Twitchen, J. Meijer, F. Kaiser, G. Balasubramanian, F. Jelezko, and J. Wrachtrup, Dynamic polarization of single nuclear spins by optical pumping of nitrogen-vacancy color centers in diamond at room temperature, *Phys. Rev. Lett.* **102**, 057403 (2009).
- [24] N. Aslam, G. Waldherr, P. Neumann, F. Jelezko, and J. Wrachtrup, Photo-induced ionization dynamics of the nitrogen vacancy defect in diamond investigated by single-shot charge state detection, *New J. Phys.* **15**, 013064 (2013).
- [25] J. Sakurai and J. Napolitano, *Modern Quantum Mechanics* (Pearson Education, London, 2014).
- [26] M. Zeng and E. H. Yong, Crooks fluctuation theorem in \mathcal{PT} -symmetric quantum mechanics, *J. Phys. Commun.* **1**, 031001 (2017).
- [27] S. W. Kim, T. Sagawa, S. De Liberato, and M. Ueda, Quantum Szilard engine, *Phys. Rev. Lett.* **106**, 070401 (2011).
- [28] J. Goold, M. Huber, A. Riera, L. del Rio, and P. Skrzypczyk, The role of quantum information in thermodynamics—a topical review, *J. Phys. A: Math. Theor.* **49**, 143001 (2016).
- [29] R. Kosloff and A. Levy, Quantum heat engines and refrigerators: Continuous devices, *Annu. Rev. Phys. Chem.* **65**, 365 (2014).
- [30] F. C. Binder, S. Vinjanampathy, K. Modi, and J. Goold, Quantum cell: Powerful charging of quantum batteries, *New J. Phys.* **17**, 075015 (2015).
- [31] N. M. Myers, O. Abah, and S. Deffner, Quantum thermodynamic devices: From theoretical proposals to experimental reality, *AVS Quantum Sci.* **4**, 027101 (2022).

- [32] B.-M. Xu, J. Zou, L.-S. Guo, and X.-M. Kong, Effects of quantum coherence on work statistics, *Phys. Rev. A* **97**, 052122 (2018).
- [33] K. Micadei, G. T. Landi, and E. Lutz, Quantum fluctuation theorems beyond two-point measurements, *Phys. Rev. Lett.* **124**, 090602 (2020).
- [34] K. Micadei, J. P. S. Peterson, A. M. Souza, R. S. Sarthour, I. S. Oliveira, G. T. Landi, R. M. Serra, and E. Lutz, Experimental validation of fully quantum fluctuation theorems using dynamic Bayesian networks, *Phys. Rev. Lett.* **127**, 180603 (2021).
- [35] A. J. Roncaglia, F. Cerisola, and J. P. Paz, Work measurement as a generalized quantum measurement, *Phys. Rev. Lett.* **113**, 250601 (2014).
- [36] A. E. Allahverdyan, Nonequilibrium quantum fluctuations of work, *Phys. Rev. E* **90**, 032137 (2014).
- [37] P. Solinas, H. J. D. Miller, and J. Anders, Measurement-dependent corrections to work distributions arising from quantum coherences, *Phys. Rev. A* **96**, 052115 (2017).
- [38] J. P. Hadden, J. P. Harrison, A. C. Stanley-Clarke, L. Marseglia, Y.-L. D. Ho, B. R. Patton, J. L. O'Brien, and J. G. Rarity, Strongly enhanced photon collection from diamond defect centers under microfabricated integrated solid immersion lenses, *Appl. Phys. Lett.* **97**, 241901 (2010).
- [39] P. Rembold, N. Oshnik, M. M. Müller, S. Montangelo, T. Calarco, and E. Neu, Introduction to quantum optimal control for quantum sensing with nitrogen-vacancy centers in diamond, *AVS Quantum Sci.* **2**, 024701 (2020).